










Mono- and sub-monolayer films of a high $T_{1/2}$ spin-crossover molecule on HOPG: temperature- and light-driven spin-state transition

Jorge Torres^{1,*} , Sangeeta Thakur¹ , Sascha Ossinger², Ivar Kumberg¹ , Evangelos Golias¹ , Clara W A Trommer², Sebastien E Hadjadj¹ , Marcel Walter¹ , Jendrik G rdes¹ , Jan Grunwald², Rahil Hosseinifar¹ , Chen Luo³ , Lalminthang Kipgen¹ , Florin Radu³ , Felix Tuzcek²  and Wolfgang Kuch^{1,*} 

¹ Institut f r Experimentalphysik, Freie Universit t Berlin, Arnimallee 14, 14195 Berlin, Germany

² Institut f r Anorganische Chemie, Christian-Albrechts Universit t zu Kiel, Max-Eyth-Stra e 2, 24118 Kiel, Germany

³ Helmholtz-Zentrum Berlin f r Materialien und Energie, Albert-Einstein-Stra e 15, 12489 Berlin, Germany

E-mail: jorge.torres@fu-berlin.de and kuch@physik.fu-berlin.de

Received 8 May 2025, revised 25 June 2025

Accepted for publication 16 July 2025

Published 29 July 2025



Abstract

We investigated the properties of the $[\text{Fe}\{\text{H}_2\text{B}(\text{pz})(\text{pypz})\}_2]$ spin-crossover complex deposited on highly oriented pyrolytic graphite (HOPG) by x-ray absorption spectroscopy in the temperature range from 10 to 350 K for sample thicknesses from 0.9(1) to 1.3(2) ML. The highest temperature at which light can excite the system to a long-lived metastable high-spin (HS) state (T_{LIESST}) and the temperature at which a thermal spin transition occurs ($T_{1/2}$) for the thin film samples are found as about 45 and 325 K, respectively, in agreement with the bulk values. The bulk phase has previously been studied by magnetic susceptibility measurements where it was found that two different polymorphic modifications exist. These findings suggest a potential correlation between T_{LIESST} and the high $T_{1/2}$ from the different film thicknesses of the tridentate $[\text{Fe}\{\text{H}_2\text{B}(\text{pz})(\text{pypz})\}_2]$ spin-crossover molecule, with thinner samples exhibiting lower $T_{1/2}$ values. Finally, the highest HS fraction achieved for $[\text{Fe}\{\text{H}_2\text{B}(\text{pz})(\text{pypz})\}_2]$ is 0.77 for samples of 0.9(1) and 1.1(1) ML on HOPG at 10 K and constant light irradiation.

Supplementary material for this article is available [online](#)

Keywords: spin-crossover molecules, thin films, x-ray absorption, LIESST, SOXIESST

* Authors to whom any correspondence should be addressed.



Original Content from this work may be used under the terms of the [Creative Commons Attribution 4.0 licence](#). Any further distribution of this work must maintain attribution to the author(s) and the title of the work, journal citation and DOI.

1. Introduction

Ultra-thin films of spin-crossover materials deposited on metallic or nonmetallic substrates could be useful in spintronic devices due to light-induced spin-state switching around room temperature, as long as the properties of isolated molecules as well as molecule-substrate interactions are well understood. Spin-crossover systems can change the spin state when external stimuli are applied (e.g. temperature, pressure or light) [1–4]. Figure 1 shows the representation of the singlet ($S = 0$) and quintet ($S = 2$) states for an Fe(II) spin-crossover molecule (SCM) as a function of the ligand field strength ($10Dq$). The electronic spin state of the SCM can change from a low-spin (LS) $t_{2g}^6 - e_g^0$ to a high-spin (HS) $t_{2g}^4 - e_g^2$ configuration. The latter follows from Hund's rule in the case the spin pairing energy is larger than the ligand-field splitting $10Dq$, which support the HS state. The study of the molecular structure modifications and spin-state dynamics of SCMs is fundamentally important due to their potential applications as construction blocks for writing/reading magnetic data storage [5], construction of organic solar cells [6], design of temperature or pressure signal detectors [7], or even the development of artificial bending muscles [8].

The light-induced excited spin-state trapping (LIESST) is an effect where the spin state of a SCM can be manipulated by light irradiation at low temperatures [9]. LIESST and thermally-driven spin-crossover processes have been described in the bulk and in solution [10–13]. However, it is also important to analyze the deposition of sublimable compounds on crystalline substrates (like Au(111) or highly oriented pyrolytic graphite (HOPG)), in order to find their characteristic behavior for possible spintronic applications engineered by spin-interface properties [14].

The study of SCMs supported by bidentate organoborate ligands has led to the development of analogous systems supported by tridentate organoborate ligands, after observing that the former could be sublimed on different substrates [15, 16]. However, on Au(111), the first monolayer (ML) of $[\text{Fe}(\text{H}_2\text{B}(\text{pz})_2)_2(\text{L})]$ showed dissociation into tetrahedral $[\text{Fe}(\text{H}_2\text{B}(\text{pz})_2)_2]$ and the co-ligand L (e.g. phen, phenme₄; pz = pyrazolyl) [16, 17]. In contrast, tripodal $[\text{Fe}(\text{HB}(\text{pz})_3)_2]$ compounds have been successfully deposited by vacuum sublimation onto various substrates, even on Au(111), showing the LIESST effect [18, 19]. For this reason, a linear tridentate ligand, $\text{H}_2\text{B}(\text{pz})(\text{pypz})$ (dihydro(pyrazolyl)(pyridylpyrazolyl)borate), was synthesized, and the derived $[\text{Fe}\{\text{H}_2\text{B}(\text{pz})(\text{pypz})\}_2]$ complex was analyzed in the bulk phase and thin films deposited on different substrates, where the spin-crossover properties were preserved, exhibiting LIESST and thermally-driven spin transition [20].

In order to describe the LIESST effect, the LIESST temperature (T_{LIESST}) is defined as the temperature where the second derivative of the HS fraction (γ_{HS}) vs T is minimum, while the temperature is increased with a rate of 0.3 K min^{-1} [21–23]. An empirical correlation between T_{LIESST}

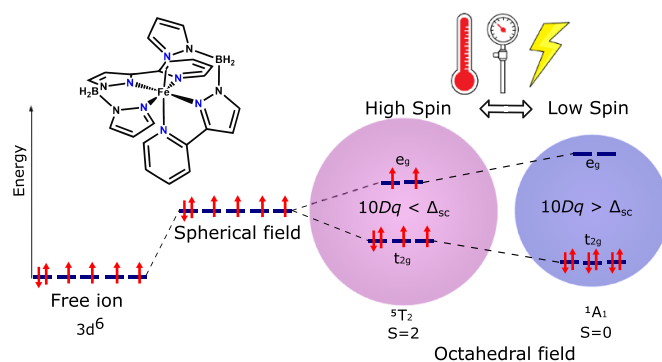


Figure 1. Ground state energy level of the free Fe(II) ion orbitals. A spherical field lifts the metal- d -orbitals, while the electrostatic repulsion between ligands and metal electrons leads to their energetic splitting. The high-spin and low-spin state can be attained by different external stimuli, affecting the relation between the ligand field strength ($10Dq$) and the spin-coupling energy (Δ_{sc}). The structure of $[\text{Fe}\{\text{H}_2\text{B}(\text{pz})(\text{pypz})\}_2]$ is shown (inset).

and $T_{1/2}$ has been found as:

$$T_{\text{LIESST}} = T_0 - 0.3T_{1/2} \quad (1)$$

where $T_{1/2}$ is the thermal transition temperature (where HS and LS states are present in a 1:1 ratio) and T_0 is defined as a temperature constant related to the denticity of the involved ligands. The 0.3 factor has been obtained as a result from different works on SCM [24–26]. It also has been found that the heating rate (θ) influences the determination of T_{LIESST} by shifting it to larger T_{LIESST} at higher heating rates [22], while at low θ rates, $T_{1/2}$ should not change.

On the other hand, the relaxation of the LIESST metastable HS state at low temperatures is expressed as $k_{\text{HL}}(T \rightarrow 0)$, where k_{HL} is the HS-LS relaxation rate constant. In some compounds a very fast spin-driven dynamic process with high transition rates between 10^6 and 10^8 s^{-1} is present [27–29]. For some other Fe(II) compounds, a very slow relaxation with long relaxation time constants ($\tau > 10$ days) has been measured [30]. One way to estimate k_{HL} is to consider the relaxation kinetics at the lowest possible temperature (e.g. 10 K) and take them as the lower limit. In the high-temperature region, the LIESST relaxation follows an *Arrhenius* behavior which can be attributed to non-adiabatic multiphonon transitions from the thermally excited vibrational levels of the HS state [22]. The thermal HS decay rate is given by:

$$k_{\text{HL}} = k_{\infty} e^{-\frac{E_a}{k_B T}} \quad (2)$$

where k_{∞} is the *Arrhenius* pre-exponential factor, E_a is the activation energy, k_B is the Boltzmann constant and T is the temperature. For a non-cooperative system, the isothermal relaxation of γ_{HS} is described by a single exponential, while for cooperative systems a sigmoidal characteristic is usually followed [31, 32]. Cooperative effects originate from elastic

interactions between nearest neighbors of a SCM in a crystal environment [33, 34]. Alternatively, results regarding the temperature dependence of the spin relaxation under constant illumination have been obtained from different experiments [35].

For various sublimable molecules deposited on a HOPG substrate, the thermally driven spin transition and the LIESST effect have been successfully observed, where total or partial switching could be detected [36–38]. In the present work, we measure these interactions for the vacuum-sublimable $[\text{Fe}\{\text{H}_2\text{B}(\text{pz})(\text{pypz})\}_2]$ SCM compound on films with different thicknesses deposited on HOPG, by means of x-ray absorption spectroscopy (XAS). In a previous study, it was found that the bulk powder of this compound exhibits two polymorphic modifications, in which phase **I** has a $T_{1/2} = 270$ K and phase **II** a $T_{1/2} = 390$ K ($\pi - \pi$ stacking/cooperativity effects vs no stacking/cooperativity effects) [20]. These results will help to describe the thickness-dependent transition temperature found for the deposited samples of $[\text{Fe}\{\text{H}_2\text{B}(\text{pz})(\text{pypz})\}_2]$ on HOPG which were subject to temperature variation and light illumination. In general, XAS results showed a $T_{1/2}$ around room temperature for the thin films as well as for the bulk sample, while almost the same T_{LIESST} (around 45 K) was determined from all samples.

2. Methodology

The synthesis of the SCM complex is described in a previous report [20], where measurements by superconducting quantum interference device (SQUID), Mößbauer, UV–Vis, Raman spectroscopy, x-ray powder diffraction and differential calorimetric analysis were performed. In this section we describe the XAS experimental setup for the SCM measurements.

2.1. X-ray absorption spectroscopy

XAS spectra were measured at the VEKMAG end-station of the beamline PM2 of the synchrotron radiation facility BESSY II [39], in a measurement chamber with a nominal pressure around 10^{-10} mbar. Before the XAS measurements, thin layers of the compound were deposited in a contiguous preparation chamber at a pressure of 10^{-9} mbar. The substrates used for the deposition of thin films are HOPG (bought from Momentive Technologies). For the bulk-phase analysis a small piece of pristine indium foil was mounted on a molybdenum sample holder and an amount around 10 mg of the sample was uniformly crimped over the indium foil and transferred directly to the measurement chamber. The HOPG substrates were freshly cleaved with help of a carbon tape inside a load-lock cleaving stage at 10^{-8} mbar and set afterwards to liquid nitrogen temperature. The molecules were sublimated at 428 K while the deposited material was measured with help of a quartz crystal microbalance mounted in front of the molecule evaporator. The measured samples thicknesses are 0.9(1), 1.1(1) and 1.3(2) ML. The thicknesses of the samples were estimated from a previous work on another Fe(II)-derived complex, where a thin film of $[\text{Fe}\{\text{H}_2\text{B}(\text{pz})_2\}_2(\text{phen})]$ (phen = 1,10-phenanthroline) SCM was deposited on HOPG and

measured stepwise *in-situ* while the final thickness was compared to XAS and scanning tunneling microscopy (STM) results of an Fe(II) octaethylporphyrin (Cl)/Cu(001) sample with thickness dimensions on a nanometer scale [36, 37, 40]. Each pristine substrate was measured before deposition of the SCM to get the background signal for the XAS analysis and check for possible contaminations. After molecule deposition, the samples were transferred to the measurement chamber and set into position for x-ray measurements at normal (90°) and magic-angle (54.7°) incidence. The x-ray light utilized was linearly *p*-polarized with a photon flux of approximately 1.6×10^9 photons $\text{s}^{-1} \text{mm}^{-2}$. The LED used for excitation has a wavelength of 520 nm with a flux density estimated as $4.2(8) \times 10^{14}$ photons $\text{s}^{-1} \text{mm}^{-2}$ at the sample position.

3. Results

This section shows the analysis of XAS spectra of $[\text{Fe}\{\text{H}_2\text{B}(\text{pz})(\text{pypz})\}_2]$ samples in the bulk phase and depositions of 0.9(1), 1.1(1) and 1.3(2) ML on HOPG, at different temperature ranges and light irradiation exposure times. While the bulk material and thin films with thicknesses of 0.9(1)- and 1.3(2)-ML were measured from a first synthesized batch, the 1.1(1)-ML film was measured from a second batch of the complex. All XAS spectra of the Fe L_3 edge, as shown in figures S1–S4 of the supplementary information (SI), show the identical shape of the HS and LS components in bulk and (sub-)ML samples, such that intact deposition of the molecules can be concluded with an upper bound of 5% of damaged molecules.

3.1. Temperature dependence without light irradiation

We first examine the thermally driven spin-crossover properties of $[\text{Fe}\{\text{H}_2\text{B}(\text{pz})(\text{pypz})\}_2]$. The temperature of the bulk, 1.1(1)- and 0.9(1)-ML samples is changed from 10 to 350 K at a constant rate, without light illumination, and every 10–20 K temperature intervals the respective XAS spectra are measured. These, and also data from previous samples measured by SQUID [20], are shown for comparison in figure 2, where γ_{HS} as a function of temperature shows different behavior for each sample. This is in part because each sample was treated with different initial conditions before XAS measurements. For example, in the case of the bulk sample, the first spectrum is measured at 10 K after a previous HS decay experiment, while the first measurement for the 0.9(1)-ML sample was taken just after the light was turned off at the end of a LIESST experiment. The HS decay experiment is just the measurement of the relaxation of γ_{HS} as a function of time while no external stimuli is applied on the molecule. Conversely, for the 1.1(1)-ML sample, the temperature was increased to 180 K and then cooled back to 10 K, in order to start measuring from the LS state. Note that the different starting conditions at lowest temperature only affect the behavior in the temperature regime of thermal relaxation of the metastable HS state, up to about 100 K. The curves from 10 to 100 K (dashed lines) are fits to describe the thermal decay of the metastable low-temperature

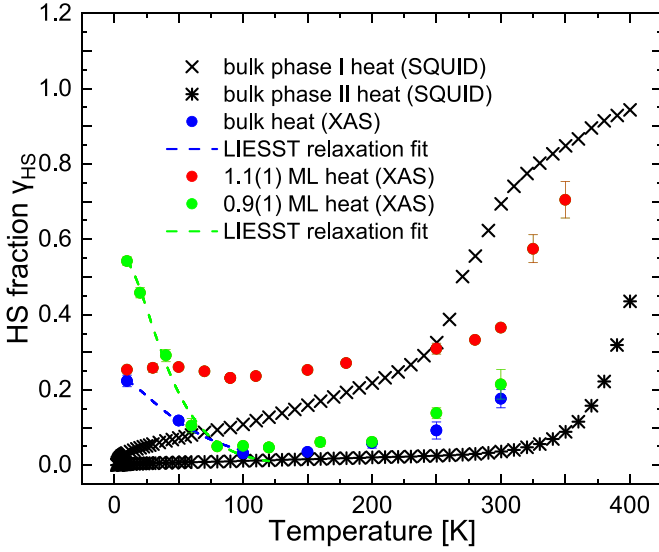


Figure 2. γ_{HS} as a function of temperature without light illumination. Temperature of bulk and 0.9(1)-ML samples increases from 10 to 300 K (blue and green dots, respectively), while for the 1.1(1)-ML sample the temperature is increased up to 350 K (red dots). Values from the bulk phase **I** and **II** samples are SQUID measurements taken from literature [20]. The low-temperature data are fitted using the LIESST relaxation equation (3) with τ^{-1} set to zero (dashed lines).

HS state without light illumination, which are described in section 3.4.

The bulk phase **I** and **II** in figure 2 are SQUID data from the literature [20]. The transition temperature $T_{1/2}$ from phase **I** is 270 K [20]. The transition temperature obtained from differential scanning calorimetry (DSC) measurements of a bulk phase **II** sample (390 K) correlates to samples with higher cooperative response, while phase **I** describes lower cooperativity. The slope of γ_{HS} with temperature of bulk phase **I** at T below 250 K points towards a cooperative behavior with temperature- or γ_{HS} -dependent cooperativity. In the case of the 1.1(1)-ML sample, as observed in figure 2, the behavior indicates a less cooperative system, closer to the bulk phase **I** sample measured by SQUID. For the bulk and 0.9(1)-ML samples measured by XAS, an intermediate behavior (between **I** and **II**) with a gradual increase of γ_{HS} as a function of temperature is present. Different contaminations of the molecular powders prepared for 0.9(1) ML, as compared to the second batch used for preparation of 1.1(1) ML, could have also influenced the amount of switchable molecules.

Independently of the initial γ_{HS} measured at 10 K for all the samples in figure 2, a near complete zero HS value could be reached around 100 K for the bulk and 0.9(1)-ML samples, while the 1.1(1)-ML sample reached a value close to 0.2 HS at this temperature. For the 0.9(1)-ML sample, the initial HS fraction at 10 K is 0.54 and for the bulk sample 0.22. In the case of the 1.1(1)-ML sample, the initial γ_{HS} fraction is 0.25 (no previous LIESST) at low temperature. However, for the 1.1(1)-ML sample at 350 K, the HS fraction obtained was the highest of all the samples at this temperature (0.7) and the

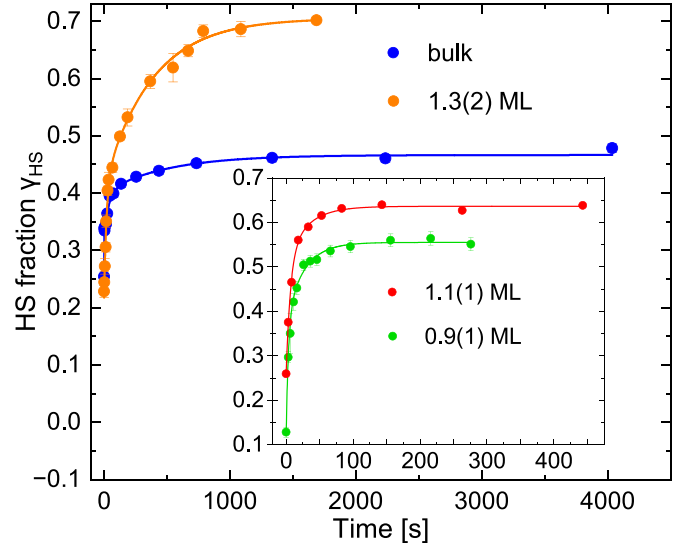


Figure 3. High-spin fraction γ_{HS} as a function of light irradiation time from LIESST of the bulk material and thin films with thicknesses of 1.3(2), 1.1(1) and 0.9(1) ML along with exponential fits. For all the samples a bi-exponential fit is used. The inverse of all the calculated time constants (τ^{-1}) are obtained from the relative fraction γ_{HS} of each sample and are shown in table S1. Respective XAS spectra are shown in SI figure S1.

experiment in general, because there was no other measurement done at this temperature for another sample. Finally, the XAS spectra of all the measured samples subject to temperature change without light illumination are shown in figure S3 of the SI.

3.2. LIESST

To carry out the LIESST experiment, the temperature of the sample is first decreased to 10 K. Then, a set of XAS measurements is performed before light irradiation. Subsequently, light is irradiated on the sample for a determined time interval and XAS spectra are measured after each irradiation period. The duration of illumination time is increased after each measurement. In figure 3, γ_{HS} as a function of light irradiation time is shown.

The XAS spectra from the LIESST experiments can be seen in figure S1 of the SI. A multiexponential fit generalizes the single exponential fit case by including additional terms that account for more complex systems, where different exponential components contribute to the overall behavior of the experimental data. While a single exponential fit represents data with a single decay constant, often used for simpler systems or when data does not exhibit significant complexity, a multiexponential fit involves a linear combination of multiple exponential functions, allowing for a more accurate representation of complex datasets, such as those arising in physical and chemical experiments [41]. The fitting process in figure 3 is carried out using the expression from equation (S2) in SI, which is composed by a pre-exponential term, or amplitude, A_n and a time constant τ_n , characteristic for a determined behavior of the measured sample.

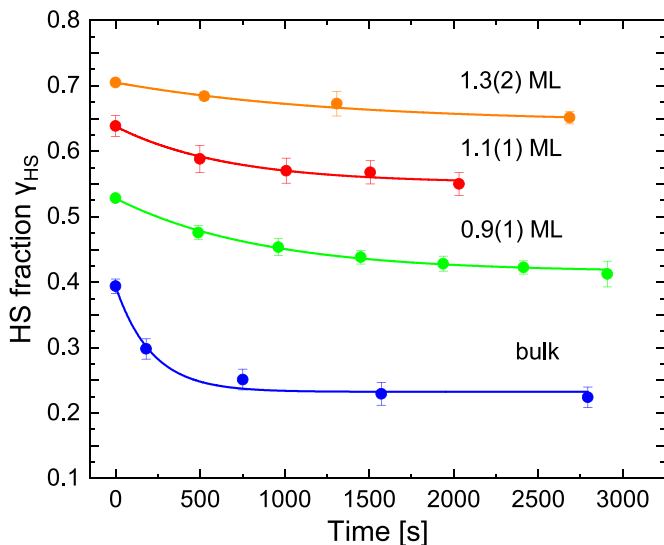


Figure 4. γ_{HS} as a function of time without light illumination for the bulk (blue), 1.3(2)- (orange), 1.1(1)- (red) and 0.9(1)- (green) ML samples at a fixed temperature of 10 K.

For each sample, two exponential terms are used to describe the γ_{HS} increase in the LIESST experiment. The HS fraction increase as a function of light irradiation time for all the samples is satisfactorily described by a double-exponential fit, where the obtained time constants seem to be also thickness-dependent. The multi-exponential fits could be related to the number of species (i.e. the assigned ground state or excited molecules) present in the sample [42]. The 0.9(1)- and 1.1(1)-ML samples seem to reach saturation faster than the other two samples, but have not been measured to longer times. It also should be noted that the x-ray beam can induce LS \rightarrow HS or HS \rightarrow LS transitions at low temperatures, a process termed as soft x-ray-induced excited spin-state trapping (SOXIESST), and reverse-SOXIESST, respectively [43, 44]. SOXIESST is analogous to LIESST in the sense that both induce an increase in γ_{HS} , but with different intensities. As concluded from a larger SOXIESST cross section than the LIESST cross section, the spin-state transition originates from secondary electron scattering in SOXIESST, rather than direct optical excitation of electronic states [44].

3.3. Metastable HS state relaxation

After HS saturation by LIESST at 10 K, the spin-state relaxation process is measured for the bulk, 1.3(2)-, 1.1(1)- and 0.9(1)-ML samples without light irradiation. After determined time intervals, XAS spectra are measured. Up to the maximum time of 2000–3000 s, the HS fraction of each sample reduces only little, as seen in figure 4. The γ_{HS} relaxation for all the samples can be described by a single-exponential decay fit. The time constants obtained from these fits are 210(50), 1320(340), 660(230), and 860(80) s for the bulk, 1.3(2)-, 1.1(1)-, and 0.9(1)-ML samples, respectively. We assume that they may correspond to an initial decay rate. The larger relaxation rate of the bulk sample could be due to low light penetration during LIESST, such that only near-surface regions

are excited. In other cases, for the solid-state compounds of $[\text{Fe}\{\text{H}_2\text{B}(\text{pz})_2\}_2(\text{phen})]$ and $[\text{Fe}\{\text{H}_2\text{B}(\text{pz})_2\}_2(\text{bipy})]$, a fast relaxation rate has been measured only at temperatures close to T_{LIESST} , and the measurements on sub-MLs of these complexes show enhanced tunneling at low temperature due to a reduced energy barrier between the metastable HS and LS states, increasing the relaxation rate relative to the bulk sample [45, 46]. Another factor that could influence the almost constant γ_{HS} after relaxation of each sample is the presence of the SOXIESST effect. The relaxation times (t_r) and the initial and final γ_{HS} values obtained at $t = 0$ and $t = t_r$, respectively, together with the fit parameters, are shown in table S3, while the conversion rates ($k_{\text{HL}}(T \rightarrow 0)$) are shown in table 1.

3.4. Temperature change at constant illumination

The simultaneous temperature change at constant light irradiation for the $[\text{Fe}\{\text{H}_2\text{B}(\text{pz})(\text{pypz})\}_2]$ bulk, 1.3(2)-, 1.1(1)- and 0.9(1)-ML samples are measured by first irradiating light at 10 K until the HS state is again saturated. Under continuous light irradiation, the temperature is increased at a constant rate (between 0.012 and 0.024 K s $^{-1}$ for heating and between 0.014 and 0.021 K s $^{-1}$ for cooling, as observed from fits of the temperature as a function of time in figure S6 of the SI). Every 10–20 K temperature intervals, x-ray absorption spectra are measured. This is continued until the metastable HS fraction has thermally relaxed and a maximum of the LS state is reached, as seen in figure 5. The temperature is varied from 10 K until 120 or 130 K, and decreased to 10 K afterwards. It is important to maintain a fixed temperature change rate, because this could influence the final HS fraction of the sample as described in detail in previous works [47], where at high heating rates the measured HS fraction resulted in higher values, thus the T_{LIESST} would shift to higher temperatures. Figure S2 from the SI shows the XAS spectra. In order to describe γ_{HS} as a function of temperature under constant illumination in a non-cooperative system, the LIESST relaxation equation can be described as [48]:

$$\frac{d\gamma_{\text{HS}}}{dT} = \left(\frac{1}{\theta}\right) \left(\tau^{-1} - \gamma_{\text{HS}}[T] \times \left(\tau^{-1} + k_{\text{HL}}(T \rightarrow 0) + k_{\infty} e^{-\frac{E_a}{k_B T}} \right) \right) \quad (3)$$

where θ is the temperature change rate, $\gamma_{\text{HS}}[T]$ is the HS fraction as a function of temperature, τ^{-1} is the inverse LIESST time constant and $k_{\text{HL}}(T \rightarrow 0)$ is the low-temperature tunneling rate. The last expression from the r.h.s of equation (3) is described by the thermal HS decay rate given by equation (2).

The relaxation curves from figure 5 are fitted using equation (3). The slope of the fit curve is obtained as the first derivative, which is represented by the curves on the top of each graph of the figure. The minima of the first derivative, indicated by the vertical lines, are related to T_{LIESST} . The derivative-curve minima for the heating process of all the samples lie around 46 to 51 K (with an average of 48 K), while for the cooling process the minima are at a slightly lower temperature compared to heating. In particular, the bulk

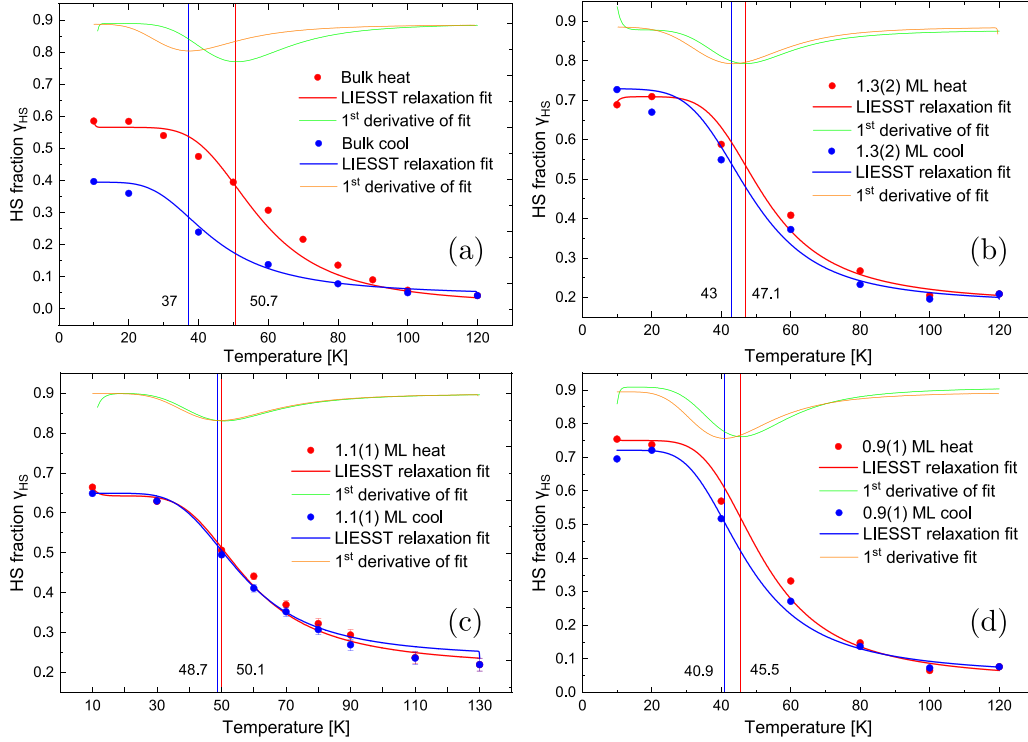


Figure 5. High-spin fraction as a function of temperature at constant illumination for (a) bulk, (b) 1.3(2)-, (c) 1.1(1)- and (d) 0.9(1)-ML samples while heating (red circles) and cooling (blue circles). The fit curves (in the respective colors) are obtained with equation (3). The curves at the top are the first derivatives of the fits (green for heating and orange for cooling), while their minima indicate T_{LIESST} as shown by the vertical lines.

Table 1. Empirical and modified inverse time constant (τ^{-1}) and HS decay rate ($k_{\text{HL}}(T \rightarrow 0)$) values from the LIESST and HS relaxation experiments at 10 K, respectively. The optimized parameters are used to fit the HS fraction as a function of temperature at constant illumination for the bulk, 1.3(2)-, 1.1(1)- and 0.9(1)-ML samples while heating and cooling as seen in figure 5. The modified values are obtained from the variance minimization using a least-squares method. The temperature change rates at constant illumination (θ) for heating and cooling are kept fixed. Dashes indicate that the values are the same as the empirical results.

Samples	Empirical values			Modified values	
	θ [Ks ⁻¹]	τ^{-1} [s ⁻¹]	$k_{\text{HL}}(T \rightarrow 0)$ [s ⁻¹]	τ^{-1} [s ⁻¹]	$k_{\text{HL}}(T \rightarrow 0)$ [s ⁻¹]
Heating					
bulk	0.0124(4)	0.002(2)	0.005(1)	0.031(1)	0.001(1)
1.3(2) ML	0.024(1)	0.0026(4)	0.0008(2)	0.02(1)	—
1.1(1) ML	0.019(1)	0.032(3)	0.0015(8)	0.008(1)	—
0.9(1) ML	0.022(1)	0.038(9)	0.0012(1)	—	—
Cooling					
bulk	-0.0143(3)	0.002(2)	0.005(1)	0.008(1)	—
1.3(2) ML	-0.0210(4)	0.0026(4)	0.0008(2)	0.005(1)	0.0002(1)
1.1(1) ML	-0.015(1)	0.032(3)	0.0015(8)	0.01(1)	—
0.9(1) ML	-0.0161(5)	0.038(9)	0.0012(1)	—	—

sample has the lowest T_{LIESST} when cooling. However, in this sample γ_{HS} after cooling does not correspond to the value before heating. A reason for this could be a lower light penetration distance in bulk crystals compared to the crystal length ($0.08 \times 0.15 \times 0.22 \text{ mm}^3$) [20], together with a slightly larger cooling rate θ compared to heating, leading to inhomogeneous excitation dynamics, which introduces a gradient of temperature along the crystal thickness [49]. Another reason could

be a thermal contraction of the sample manipulator, changing the measurement spot location on the spatially inhomogeneous powder sample. However, the latter assumption could imply only a change in the spectra intensity and not necessarily a different HS fraction. Nevertheless, including this value of T_{LIESST} , the cooling T_{LIESST} is found between 37 and 49 K, with an average of 42 K. The obtained T_{LIESST} temperatures are shown in table 2, and are similar to other Fe(II) complexes

Table 2. Pre-exponential factor k_∞ and activation energy E_a/k_B obtained from the fit of the HS fraction as a function of temperature at constant illumination for heating and cooling of the bulk, 1.3(2)-, 1.1(1)- and 0.9(1)-ML samples shown in figure 5, using equation (3) and the optimized values from table 1. T_{LIESST} for both heating and cooling is also shown, which is obtained from the first derivative curves on top of the fitted graphs from figure 5.

Samples	Heating			Cooling		
	k_∞ [s ⁻¹]	E_a/k_B [K]	$T_{\uparrow\text{LIESST}}$ [K]	k_∞ [s ⁻¹]	E_a/k_B [K]	$T_{\downarrow\text{LIESST}}$ [K]
bulk	5.4(2)	295(1)	50.7(1)	0.6(1)	171(13)	37.0(5)
1.3(2) ML	3(1)	263(3)	47.1(5)	1.13(5)	274(10)	43.0(7)
1.1(1) ML	0.85(3)	266(6)	50(2)	1.4(4)	275(33)	49(3)
0.9(1) ML	3.6(7)	235(2)	45.5(7)	2.8(5)	205(3)	41(1)

Table 3. Empirical and modified parameters obtained from the HS fraction as a function of temperature without light illumination for the bulk and 0.9(1)-ML samples between 10 and 100 K as shown in figure 2 (dashed lines). The k_∞ and E_a/k_B values are obtained by approximating equation (3) and setting τ^{-1} equal to zero, while θ_{heat} is kept fixed.

Sample	Empirical values		Modified values	Approximated values		
	θ_{heat} [Ks ⁻¹]	$k_{\text{HL}}(T \rightarrow 0)$ [s ⁻¹]	$k_{\text{HL}}(T \rightarrow 0)$ [s ⁻¹]	k_∞ [s ⁻¹]	E_a/k_B [K]	T_{LIESST} [K]
bulk	0.05(2)	0.005(1)	0.0009(1)	0.03(13)	207(145)	52(15)
0.9(1) ML	0.023(2)	0.0012(1)	0.0004(1)	0.01(4)	126(82)	42(6)

supported by tridentate ligands (e.g. $[\text{Fe}(\text{bpp})_2]\text{Br}_2 \cdot 5\text{H}_2\text{O}$ with $T_{\text{LIESST}} = 40$ K and $[\text{Fe}(\text{pap})_2]\text{PF}_6 \cdot \text{MeOH}$ with 55 K) [25, 50]. The non-monotonic behavior as a function of coverage could be explained by the rearrangement of molecules on the substrate, a possible influence of the second layer over the first layer underneath (in the case of multilayers) or the influence of molecule-substrate interactions.

In the case of the curves from 10 to 100 K in figure 2 (dashed lines), these are fitted using the LIESST relaxation equation (3) with τ^{-1} set to zero. For this, $k_{\text{HL}}(T \rightarrow 0)$ was modified by a least-squares minimization between the experimental data and the fitted curves, while the temperature change rate was kept fixed (as described below). The LIESST relaxation values in table 3 show T_{LIESST} values of the bulk and 0.9(1)-ML samples from figure 2 which lay slightly below the T_{LIESST} of other Fe(II) SCM powder samples found in the literature (55 K) [50]. Comparing the pre-exponential factor (k_∞) and the activation energy term (E_a/k_B) values from tables 2 and 3, they look the same, but in particular k_∞ values from table 3 are more similar to lower range values (approximately 10^{-2}s^{-1}) from other complexes found in the literature [36, 38, 51]. Finally, E_a/k_B approximates to common activation energies of different compounds which can vary from zero to 1390 K (0–2000 cm⁻¹) while changing the temperature in the range from 10 to 150 K [51]. For fitting the relaxation curves of figure 5 using equation (3), the LIESST inverse time constant τ^{-1} and temperature-independent HS decay rate $k_{\text{HL}}(T \rightarrow 0)$ should be the same as obtained from the respective LIESST and HS relaxation experiments described above, so that the parameters k_∞ and E_a/k_B can be obtained. However, in order to fit the curves with the lowest deviation possible, some of the empirical values (from both τ^{-1} and $k_{\text{HL}}(T \rightarrow 0)$) had to be modified using a least-square method. To observe the influence of the deviation minimization of the empirical kinetic parameters, a methodical modification is carried out in figure S5, based on τ^{-1} and $k_{\text{HL}}(T \rightarrow 0)$ of the 1.1(1)- and 1.3(2)-ML samples,

respectively. This modification can be compared with the work done on a weakly cooperative iron(II) SCM [22], where a systematic modification of the $k_{\text{HL}}(T \rightarrow 0)$ rate is carried out and a change of an abrupt γ_{HS} slope to a more gradual steepness is observed while changing from a small ($1.2 \times 10^{-5}\text{s}^{-1}$) to a higher ($3.1 \times 10^{-4}\text{s}^{-1}$) value of $k_{\text{HL}}(T \rightarrow 0)$. These results are similar to the 1.3(2)-ML sample cooling in figure S5(d), where a $k_{\text{HL}}(T \rightarrow 0)$ value is optimized from $8(2) \times 10^{-4}$ to $2.0(2) \times 10^{-4}\text{s}^{-1}$. It can be seen that smaller values of $k_{\text{HL}}(T \rightarrow 0)$ give larger steepness. Inversely, in the case of the τ^{-1} optimization, larger rate constants increase the steepness of γ_{HS} , for both heating and cooling.

In table 1 the respective empirical and modified values of τ^{-1} and $k_{\text{HL}}(T \rightarrow 0)$ used for fitting the heating and cooling γ_{HS} curves in figure 5 are shown. Table 2 shows the approximated k_∞ and E_a/k_B values obtained from fitting the thermal HS decay term in equation (3). The E_a values are similar to the typical Fe(II) SCM activation energies from literature (170 to 240 cm⁻¹) [45]. For example, the obtained E_a/k_B values for the 1.3(2)-ML sample are 263(3) and 274(19) K (183(2) and 190(13) cm⁻¹) for heating and cooling, respectively. A high E_a/k_B value, e.g. while heating the bulk sample (295(1) K), indicates a more stable light-temperature-induced HS state [38]. Thin-film samples have similar activation energies for both heating and cooling cycles.

In the case of k_∞ , all pre-exponential terms are found around $1\text{--}5\text{s}^{-1}$, which is 6–9 orders of magnitude lower than values from some complexes [30, 52], but similar to others [22]. Moreover, by comparing the 1.3(2)- and 1.1(1)-ML samples seen in figures 5(b) and (c), both reach the lowest value of 0.2 HS around 120 K, which could be due to a locked HS species at depositions of multilayer arrangements. Nevertheless, it is from the 0.9(1)-ML film on HOPG at 10 K and constant light irradiation that, compared to a completely switching $[\text{Fe}\{\text{H}_2\text{B}(\text{pz})_2\}_2(\text{bipy})]$ from the literature [37], the highest HS fraction achieved for $[\text{Fe}\{\text{H}_2\text{B}(\text{pz})(\text{py})\}_2]$ is a

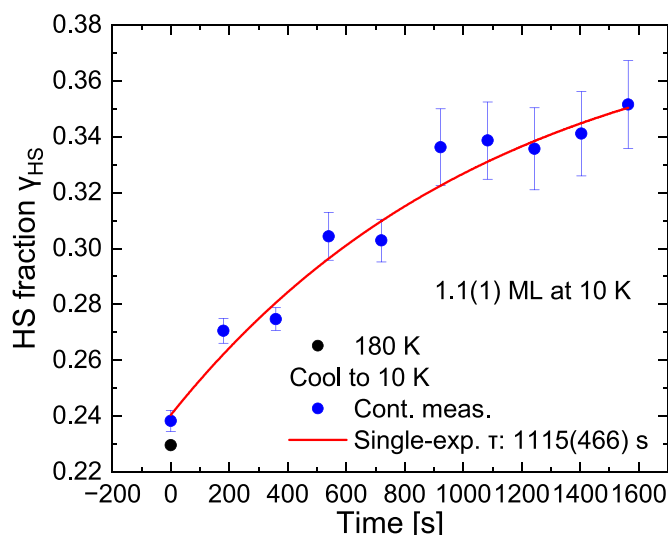


Figure 6. SOXIESST effect at 10 K during continuous XAS measurements. Shown is the HS fraction as a function of exposure time to x rays of the 1.1(1)-ML sample. It presents a γ_{HS} of 0.23 at 180 K and, after decreasing the temperature to 10 K, a γ_{HS} of 0.24 is maintained. After 10 continuous measurements, SOXIESST is observed causing an increase to 0.35 HS. The red curve represents a single-exponential fit with $\tau = 1120 \pm 470$ s.

total of 0.77 HS from the temperature change at constant light illumination experiment.

3.5. SOXIESST

As a last experiment, the sample of 1.1(1) ML thickness was subject to a set of continuous XAS measurements at 10 K.

Before the start of the experiments shown in figure 6, the 1.1(1)-ML sample exhibited a HS fraction γ_{HS} of around 0.23 at 180 K, which slightly increased to 0.24 after lowering the temperature to 10 K without light illumination. After a set of continuous measurements (10 in total with 170(10) s between each measurement and no light illumination) the HS fraction increases and a γ_{HS} of 0.35 is achieved. This can be assigned to the soft-x-ray-induced excited spin-state trapping (SOXIESST) effect, where the x-ray beam has an influence on the sample's electronic configuration [43, 44].

4. Discussion

From previous SQUID measurements of the $[\text{Fe}\{\text{H}_2\text{B}(\text{pz})(\text{pypz})\}_2]$ bulk sample obtained by Ossinger *et al* [20], it was found that $[\text{Fe}\{\text{H}_2\text{B}(\text{pz})(\text{pypz})\}_2]$ exhibits polymorphism with two slightly different crystalline modifications. One phase, denominated as **I**, shows a transition temperature of $T_{1/2} \approx 270$ K. The second polymorph (**II**) has a $T_{1/2} \approx 390$ K. On the other hand, special cooperative effects arising from $\pi - \pi$ stacking were found by single crystal structure analysis of **II** and from the isotopic zinc complex as the polymorph **I** [20]. Taking into account that both, phase **I** and **II**, were found in a bulk sample, from looking at figure 2, one is tempted to attribute

the curve measured for the 1.1(1)-ML sample to the presence of polymorphism type **I** in that sample (where $T_{1/2} \approx 325$ K). However, this sample was synthesized in a second batch and it cannot be excluded that a certain fraction of damaged non-switching molecules leads to the higher amount of molecules in the HS state at temperatures between 100 and 200 K. In the bulk samples and for the lowest coverage of 0.9(1) ML, the crystal structure type **II** apparently constitutes part of the switching behavior, as observed in figure 2. In comparison to the 1.1(1)-ML sample, the lack of measurements above 300 K for the rest of the samples prevents an estimation of $T_{1/2}$. All samples behave almost the same around 300 K, above which γ_{HS} increases abruptly for the 1.1(1)-ML sample, until the last measured point at a temperature of 350 K. Other tridentate complexes with similar transition temperatures are the $[\text{Fe}(\text{pap})_2]\text{PF}_6 \cdot \text{MeOH}$ and $[\text{Fe}(\text{bpp}_2)]\text{X}_2 \cdot n\text{H}_2\text{O}$ families with $T_{1/2}$ of 288 K and between 250 and 340 K, respectively [25, 50]. Another example is $[\text{Fe}(\text{L}_{\text{xyz}}\text{N}_5)(\text{CN})_2] \cdot n\text{H}_2\text{O}$ with a diamagnetic behavior below 420 K and a complete switch at 475 K. However, this HS state configuration is irreversible and once the temperature is increased, it is not possible to recover the LS state again, possibly due to dehydration while heating [53].

The LIESST experiment in figure 3 shows the increase of the HS state fraction as a function of light illumination time in the different samples and respective fits, presenting a multi-exponential behavior. The number of exponential terms could be related to the number of adsorbed molecular species present in the sample. Molecular species refer to HS excited electronic states where an ultrafast or a slow relaxation can occur after excitation, giving place to characteristic intra- and intermolecular interactions between the molecules and their surroundings (e.g. solvatomorphic molecules) [42]. However, a large number of intermolecular contacts would give place to large contributions of energetic interactions, but not necessarily to large cooperativities. In a recent study by Vela *et al*, it is shown that in six solvatomorphs of $[\text{Fe}^{\text{II}}(2 - \text{pic})_3]\text{Cl}_2$, cooperativity is not proportional to the strength of intermolecular interactions, but rather proportional to the temperature and the HS state of the molecules [54]. In the LIESST experiment, cooperative photo-processes are present at the time between light irradiation and the start of a new measurement, leading to a γ_{HS} relaxation, surpassed however, after several light illumination steps. LIESST has also been described as a rapid perturbation from a pulsed laser irradiation in the metal-to-ligand charge-transfer (MLCT) absorption band, affecting the equilibrium between the LS (^1A) and HS (^5T) states of Fe(II) complexes. So, upon radiation of the MLCT band, the ^5T state is formed from the initially populated charge-transfer state permitting the study of spin dynamics in a wide range of systems [55].

The isothermal relaxation of γ_{HS} without light illumination in figure 4 shows a single-exponential decay for all measured samples within the investigated time interval. The bulk sample shows the fastest rate, proving the previous LIESST assumption that thicker samples have larger saturation times due

to a faster relaxation. However, as excitation and relaxation processes take place under different principles (one through a pathway of potential electronic surfaces and the other mainly through tunneling reactions) [30, 51], excited species would be attained for longer times rather than relaxation processes. Moreover, the total waiting time of ~ 3000 s does not assert the complete relaxation of the metastable HS state, for which a longer measurement time would be needed. In the case of a $[\text{Fe}(\text{pypypyr})_2]$ bulk sample analyzed by Grunwald *et al.*, a long-lived metastable HS state at low temperatures exhibited an extrapolated half time of 781 min. when XAS data were fitted under the restriction of zero HS fraction at large times [48]. Interestingly, this relaxation, in particular, could be fitted only with a bi-exponential fit. Nevertheless, for practical purposes, we handle our results under a single-exponential approximation in order to compare the parameters from all samples of $[\text{Fe}\{\text{H}_2\text{B}(\text{pz})(\text{pypz})\}_2]$, which are, as already mentioned, improved under a least squares fit in the LIESST relaxation evaluation. Notably, $[\text{Fe}\{\text{H}_2\text{B}(\text{pz})(\text{pypz})\}_2]$ has been also analyzed by STM on a metallic surface of Ag(111), which showed a favorable spin-state transition and long-time stable γ_{HS} at low temperatures, same as with a Co(II) SCM analog [56–58].

The values found from the experiments described above are summarized in table 1, where modified and non-modified values for both inverse time constants and relaxation rate values apparently have similar orders of magnitude. In average, the thicker the sample, the larger τ^{-1} and smaller $k_{\text{HL}}(T \rightarrow 0)$ values are obtained. However, less uniformity is observed for the inverse time constants while cooling. A possible reason for the different τ^{-1} values could have arisen from the initial LIESST evaluation, which shows a multi-exponential behavior for each sample and several time constants are obtained. Because for the evaluation of the HS fraction as a function of temperature at constant light illumination in figure 5 just a single time constant value is considered using equation (3), the inverse time constant is thus modified to properly fit the measured behavior. Nevertheless, the final values lie around the typical order of magnitude from other SCM (10^{-1} – 10^{-6} s $^{-1}$) [36–38, 59, 60]. In the case of the relaxation rate, the approximations arise from a single-exponential decay equation, thus, $k_{\text{HL}}(T \rightarrow 0)$ does not change significantly (except for the cooling of the 1.3(2)-ML sample). Finally, the relaxation rates are found to be around 10^{-4} s $^{-1}$, where for a typical iron(II) SCM, rates have also been found in a wider range, from 10^7 to 10^{-7} s $^{-1}$ [13, 30]. As observed in figure 5, an average T_{LIESST} of 48 and 42 K is obtained for heating and cooling, respectively. An instability was observed while cooling the bulk sample, where cooperativity could have taken place on the low HS state conversion, due to a rapid decrease of γ_{HS} for thicker samples. Moreover, although it has been thought that strong cooperativity plays a role for large photo-induced state life-times [61], this reasoning could be rather related to some strongly cooperative materials that rarely exhibit photoswitching [62]. It is also indispensable to consider that the temperature change rate plays an important role in determining T_{LIESST} , as described by Seredyuk *et al* [63]. They measured a T_{LIESST} of 81 K without light irradiation on a bulk

sample of $[\text{Fe}(n\text{Bu} - \text{im})_3(\text{tren})](\text{PF}_6)_2$ for a heating rate of 4 K min $^{-1}$, while for a slower heating rate of 0.1 K min $^{-1}$ they found a T_{LIESST} of 53 K. They also showed that $T_{1/2}$ is related to the heating rate only if cooperativity is present, where higher rates translate into smaller $T_{1/2}$ values and inversely, slower rates show larger $T_{1/2}$ values, up to the point where hysteretic behavior is observed. However, even without cooperativity, a faster heating rate can raise $T_{1/2}$ if it is of the order of the thermal decay rate.

Comparing the results for γ_{HS} at low temperature and constant illumination from table 2 against the results obtained at low temperature with no illumination from table 3, E_a values from table 3 are in general a bit lower than the activation energies from table 2. Further, k_{∞} values are more than 2 or 3 orders of magnitude higher compared to the rates obtained via temperature change without light irradiation, as shown in table 2. The pre-exponential factor k_{∞} is the number of relaxation events per time (leading to a switching or not), and it oscillates in the order of magnitude from 10^{12} to 10^{14} s $^{-1}$, which corresponds to ~ 170 fs (molecular vibrations are normally in the time period between 10–100 fs) [64]. Thus, higher frequencies would implicate faster relaxation after excitation by light. However, our measurements are not able to cover up results with this precision. In the case of T_{LIESST} , both tables 2 and 3 show similar values for the heating process where an almost identical T_{LIESST} is obtained for both thick and thin samples. Additionally, if the association of higher $T_{1/2}$ to thicker samples applies in this range, T_{LIESST} does not seem to be affected by an inverse energy gap law due to a possible conformation of the sample between phase I and II. It can be seen in figure 2 that for the thin layers as well as the bulk sample, T_{LIESST} remains basically the same, while for the bulk sample, and interestingly the 0.9(1)-ML sample too, γ_{HS} tend to gradually describe a phase II compound behavior with a higher transition temperature.

The last part of the XAS experiments is presented in figure 6, where the SOXIESST effect is observed on the 1.1(1)-ML sample as an increase of γ_{HS} during the first 10 measurements, starting from a 0.24 HS state until saturation, achieving a final 0.35 HS. To compare the SOXIESST effect with the LIESST effect, the cross-sections of the x-ray and the visible-light photons used to excite the sample have to be compared. The cross-sections of the samples are given as $\sigma = \tau^{-1} \phi^{-1}$, where τ is the time constant and ϕ is the respective photon flux density. Thus, for the 1.1(1)-ML $\sigma_{\text{xray}} = (1115(466) \text{ s})^{-1} (1.6 \times 10^9 \text{ photons s}^{-1} \text{ mm}^{-2})^{-1} = 56(16) \text{ \AA}^2$, and $\sigma_{\text{LIESST}} = 7.7(3) \times 10^{-3} \text{ \AA}^2$. The cross-section from $[\text{Fe}\{\text{H}_2\text{B}(\text{pz})(\text{pypz})\}_2]$ has been also evaluated from vacuum ultraviolet-induced ESST (VUV-IESST) with higher values of 6 \AA^2 [65]. On the other hand, SOXIESST cross-section values of $[\text{Fe}\{\text{H}_2\text{B}(\text{pz})_2\}_2(\text{bipy})]$ of 6 \AA^2 (film sample) [44] and approximately 2 \AA^2 (bulk sample) [66] have been found, which seem to be lower than the SOXIESST cross-sections found here ($\sim 56 \text{ \AA}^2$ for 1.1(1) ML). Nevertheless, all the mentioned cross-sections lie in the same order of magnitude in comparison to the

lower LIESST cross-section, which is more similar to the cross-section values reported for the LIESST on thin films of $[\text{Fe}\{\text{H}_2\text{B}(\text{pz})_2\}_2(\text{phen})]$ and $[\text{Fe}\{\text{H}_2\text{B}(\text{pz})_2\}_2(\text{bipy})]$ on HOPG (around $0.009\text{--}0.019\text{ \AA}^2$) [36, 37], while in the case of the bulk sample (0.137 \AA^2) one has to consider other factors such as the decrease of the light intensity in the vicinity of the surface [59, 60]. In general, the different SOXIESST cross-sections describe an excited spin-state process by other means rather than direct x-ray excitation, where secondary scattered electrons from the substrate act as charge carriers in the excitation process and thus in the switching process [44, 67].

5. Conclusions

The SCM $[\text{Fe}\{\text{H}_2\text{B}(\text{pz})(\text{pypz})\}_2]$, supported by the linear tridentate ligand $\text{H}_2\text{B}(\text{pz})(\text{pypz})$, has been deposited intactly on an HOPG substrate, whereby the thermally driven spin transition and the low-temperature LIESST effect could be observed by XAS. A $T_{1/2}$ around 325 K was obtained for a 1.1(1)-ML sample, relatively similar to the bulk phase I sample (275(1) K). The HS fraction obtained from the bulk sample as a function of temperature differs somewhat from the one previously obtained by SQUID, possibly due to an interaction with the x rays, where an intermediate behavior between the phase-I and phase-II polymorphs appears to be observed. An average T_{LIESST} of 45 K was obtained from all the measured samples, which was always higher while heating the sample. In general the adsorbed MLs behave like phase-I with respect to the thermal switching ($T_{1/2}$), but do not show the gradual slope at lower temperatures, which has to be attributed to cooperativity, as the respective bulk material. The gradual increase in γ_{HS} as a function of temperature already at temperatures clearly below $T_{1/2}$ places the ML samples somewhere between the type I and type II polymorphic modifications of the bulk material.

Comparing the high transition temperatures acquired to the respective T_{LIESST} values of the samples, it seems to be in agreement with equation (1), where a $T_0 = 150\text{ K}$ related to a tridentated ligand is used to properly satisfy the relation. As shown, the spin dynamics at low temperature regimes can be described as a non-cooperative effect, while spin transitions at higher temperatures can only be described with a cooperative model. Finally, a comparison with the fully switching $[\text{Fe}\{\text{H}_2\text{B}(\text{pz})_2\}_2(\text{bipy})]$ SCM shows that the highest HS fraction (0.77 HS) was obtained for the 0.9(1)- and 1.1(1)-ML samples of $[\text{Fe}\{\text{H}_2\text{B}(\text{pz})(\text{pypz})\}_2]$ on HOPG, which could be also due to the presence of different molecular species and a fast relaxation after light irradiation. Nevertheless, the quality of the surface must be also considered.

Data availability statement

The data that support the findings of this study will be openly available at the following URL/DOI: <http://dx.doi.org/10.17169/refubium-47928>.

Acknowledgments

We acknowledge the grant of the DFG Project KU 1115/13-1 and TU 58/18-1 and the support and attention by the Helmholtz Zentrum Berlin and the beamtimes at the PM2-VEKMAG beamline at BESSY II in Berlin to realize the x-ray absorption measurements. JT wants to acknowledge the scholarship (No. 689884) from CONAHCYT and financial support by Freie Universität Berlin. Much appreciated is also the support from Dr Shinwari at the beam line station.

Conflicts of interest

The authors declare there are no conflicts of interest.

Author contributions

Jorge Torres  0009-0005-6767-3757

Data curation (equal), Investigation (equal), Visualization (lead), Writing – original draft (lead)

Sangeeta Thakur  0000-0003-4879-5650

Data curation (equal), Investigation (equal), Supervision (supporting), Writing – review & editing (equal)

Sascha Ossinger

Investigation (supporting), Writing – review & editing (equal)

Ivar Kumberg  0000-0002-3914-0604

Data curation (equal), Investigation (supporting), Writing – review & editing (supporting)

Evangelos Golias  0000-0003-1483-1959

Data curation (equal), Investigation (supporting), Supervision (supporting), Writing – review & editing (supporting)

Clara W A Trommer

Investigation (supporting), Resources (supporting), Writing – review & editing (supporting)

Sebastien E Hadjadj  0000-0002-6045-574X

Data curation (equal), Investigation (supporting), Writing – review & editing (supporting)

Marcel Walter  0009-0003-4145-0358

Data curation (equal), Investigation (equal), Writing – review & editing (supporting)

Jendrik Gordes  0000-0003-4321-8133

Data curation (equal), Investigation (supporting), Writing – review & editing (supporting)

Jan Grunwald

Investigation (supporting), Resources (supporting), Writing – review & editing (supporting)

Rahil Hosseinifar  0000-0002-9124-008X

Data curation (supporting), Investigation (supporting), Writing – review & editing (supporting)

Chen Luo  0000-0001-6476-9116

Data curation (equal), Investigation (supporting),
Methodology (supporting), Writing – review &
editing (supporting)

Lalminthang Kipgen  0000-0002-8401-4930

Conceptualization (supporting), Data curation (lead),
Investigation (equal), Writing – review & editing (supporting)

Florin Radu  0000-0003-0284-7937

Data curation (supporting), Methodology (equal),
Resources (supporting), Writing – review &
editing (supporting)

Felix Tuczek  0000-0001-7290-9553

Conceptualization (lead), Funding acquisition (lead), Project
administration (lead), Writing – review & editing (lead)

Wolfgang Kuch  0000-0002-5764-4574

Conceptualization (lead), Funding acquisition (lead),
Investigation (equal), Project administration (lead),
Supervision (lead), Writing – review & editing (lead)

References

- [1] Gütllich P, Gaspar A B and Garcia Y 2013 Spin state switching in iron coordination compounds *Beilstein J. Org. Chem.* **9** 342–91
- [2] Halcrow M A 2013 Structure: function relationships in molecular spin-crossover materials *Spin-Crossover Materials Properties and Applications* ed M A Halcrow (Wiley) pp 147–64
- [3] Gütllich P, Hauser A and Spiering H 1994 Thermal and optical switching of iron(II) complexes *Angew. Chem., Int. Ed.* **33** 2024–54
- [4] Real J A, Gaspar A B and Muñoz M C 2005 Thermal, pressure and light switchable spin-crossover materials *Dalton Trans.* 2062–79
- [5] Bousseksou A and Molnár G 2003 The spin-crossover phenomenon: towards molecular memories *C. R. Chim.* **6** 1175–83
- [6] Zhang K, Ash R, Girolami G S and Vura-Weis J 2019 Tracking the metal-centered triplet in photoinduced spin crossover of $\text{Fe}(\text{phen})_3^{2+}$ with tabletop femtosecond M-edge x-ray absorption near-edge structure spectroscopy *J. Am. Chem. Soc.* **141** 17180–8
- [7] Linares J, Codjovi E and Garcia Y 2012 Pressure and temperature spin crossover sensors with optical detection *Sensors* **12** 4479–92
- [8] Tondou B, Piedrahita-Bello M, Salmon L, Molnár G and Bousseksou A 2022 Robust linear control of a bending molecular artificial muscle based on spin crossover molecules *Sens. Actuators A* **335** 113359
- [9] Decurtins S, Gütllich P, Köhler C P, Spiering H and Hauser A 1984 Light-induced excited spin state trapping in a transition-metal complex: the hexa-1-propyltetrazole-iron (II) tetrafluoroborate spin-crossover system *Chem. Phys. Lett.* **105** 1–4
- [10] Decurtins S, Gütllich P, Köhler C P and Spiering H 1985 New examples of light-induced excited spin state trapping (LIESST) in iron(II) spin-crossover systems *J. Chem. Soc. Chem. Commun.* 7 430–2
- [11] Decurtins S, Gütllich P, Hasselbach K M, Hauser A and Spiering H 1985 Light-induced excited-spin-state trapping in iron(II) spin-crossover systems. Optical spectroscopic and magnetic susceptibility study *Inorg. Chem.* **24** 2174–8
- [12] Hauser A 1986 Reversibility of light-induced excited spin state trapping in the $\text{Fe}(\text{ptz})_6(\text{BF}_4)_2$ and the $[\text{Zn}_{1-x}\text{Fe}_x(\text{ptz})_6](\text{BF}_4)_2$ spin-crossover systems *Chem. Phys. Lett.* **124** 543–8
- [13] Hauser A, Vef A and Adler P 1991 Intersystem crossing dynamics in Fe(II) coordination compounds *J. Chem. Phys.* **95** 8710–7
- [14] Kipgen L, Bernien M, Tuczek F and Kuch W 2021 Spin-crossover molecules on surfaces: from isolated molecules to ultrathin films *Adv. Mater.* **33** 14
- [15] Naggert H, Rudnik J, Kipgen L, Bernien M, Nickel F, Arruda L M, Kuch W, Näther C and Tuczek F 2015 Vacuum-evaporable spin-crossover complexes: physicochemical properties in the crystalline bulk and in thin films deposited from the gas phase *J. Mater. Chem. C* **3** 7870–7
- [16] Ossinger S et al 2017 Vacuum-evaporable spin-crossover complexes in direct contact with a solid surface: bismuth versus gold *J. Phys. Chem. C* **121** 1210–9
- [17] Gopakumar T G et al 2013 Spin-crossover complex on Au(111): structural and electronic differences between mono- and multilayers *Chem. Eur.* **19** 15702–9
- [18] Davesne V et al 2015 Hysteresis and change of transition temperature in thin films of $\text{Fe}[\text{Me}_2\text{Pyrz}]_3\text{BH}_2$, a new sublimable spin-crossover molecule *J. Chem. Phys.* **142** 194702
- [19] Bairagi K et al 2018 Temperature-, light- and soft x-ray-induced spin crossover in a single layer of Fe^{II} -pyrazolylborate molecules in direct contact with gold *J. Chem. Phys. C* **122** 727–31
- [20] Ossinger S, Näther C, Buchholz A, Schmidtman M, Mangelsen S, Beckhaus R, Plass W and Tuczek F 2020 Spin transition of an iron(II) organoborate complex in different polymorphs and in vacuum-deposited thin films: influence of cooperativity *Inorg. Chem.* **59** 7966–79
- [21] Létard J-F, Guionneau P, Rabardel L, Howard J A K, Goeta A E, Chasseau D and Kahn O 1998 Structural, magnetic and photomagnetic studies of a mononuclear iron(II) derivative exhibiting an exceptionally abrupt spin transition. Light-induced thermal hysteresis phenomenon *Inorg. Chem.* **37** 4432–41
- [22] Létard J-F, Chastanet G, Nguyen O, Marcén S, Marchivie M, Guionneau P, Chasseau D and Gütllich P 2003 Spin crossover properties of the $[\text{Fe}(\text{PM} - \text{BiA})_2(\text{NCS})_2]$ complex—phases I and II *Monatsh. Chem.* **134** 165–82
- [23] Chastanet G, Desplanches C, Baldé C, Rosa P, Marchivie M and Guionneau P 2018 A critical review of the T(LIESST) temperature in spin crossover materials — what it is and what it is not *Chem. Sq.* **2** 18
- [24] Létard J-F, Guionneau P, Nguyen O, Sánchez Costa J, Marcén S, Chastanet G, Marchivie M and Goux-Capes L 2005 A guideline to the design of molecular-based materials with long-lived photomagnetic lifetimes *Chem. Eur. J.* **11** 4582–9
- [25] Marcén S, Lecren L, Capes L, Goodwin H A and Létard J-F 2002 Critical temperature of the LIESST effect in a series of hydrated and anhydrous complex salts $[\text{Fe}(\text{bpp})_2]\text{X}_2$ *Chem. Phys. Lett.* **358** 87–95
- [26] Shimamoto N, Ohkoshi S, Sato O and Hashimoto K 2002 Control of charge-transfer-induced spin transition temperature on cobalt-iron Prussian blue analogues *Inorg. Chem.* **41** 678–84
- [27] Dose E V, Hoselton M A, Sutin N, Tweedle M F and Wilson L J 1978 Dynamics of intersystem crossing processes in solution for six-coordinate d^5 , d^6 and d^7 spin-equilibrium metal complexes of iron(III), iron(II) and cobalt(II) *J. Am. Chem. Soc.* **100** 1141–7

- [28] Adler P, Hauser A, Vef A, Spiering H and Gütlich P 1989 Dynamics of spin state conversion processes in the solid state *Hyp. Interact.* **47** 343–56
- [29] Brady C, McGarvey J J, McCusker J K, Toftlund H and Hendrickson D N 2004 Time-resolved relaxation studies of spin crossover systems in solution *Spin Crossover in Transition Metal Compounds III* ed P Gütlich and H A Goodwin (Springer) pp 1–22
- [30] Hauser A 2004 Light-induced spin crossover and the high-spin \rightarrow low-spin relaxation *Top. Curr. Chem.* **234** 155–98
- [31] Boukheddaden K, Shteto I, Hôo B and Varret F 2000 Dynamical model for spin-crossover solids. I. Relaxation effects in the mean-field approach *Phys. Rev. B* **62** 14796–805
- [32] Nicolazzi W and Pillet S 2012 Structural aspects of the relaxation process in spin crossover solids: phase separation, mapping of lattice strain and domain wall structure *Phys. Rev. B* **85** 13
- [33] Bousseksou A, Molnár G, Salmon L and Nicolazzi W 2011 Molecular spin crossover phenomenon: recent achievements and prospects *Chem. Soc. Rev.* **40** 3313–35
- [34] Pavlik J and Boča R 2013 Established static models of spin crossover *Eur. J. Inorg. Chem.* **5–6** 697–709
- [35] Nicolazzi W and Bousseksou A 2018 Thermodynamical aspects of the spin crossover phenomenon *C. R. Chim.* **21** 1060–74
- [36] Bernien M *et al* 2015 Highly efficient thermal and light-induced spin-state switching of an Fe(II) complex in direct contact with a solid surface *ACS Nano* **9** 8960–6
- [37] Kipgen L *et al* 2018 Evolution of cooperativity in the spin transition of an iron(II) complex on a graphite surface *Nat. Commun.* **9** 8
- [38] Thakur S *et al* 2021 Thermal- and light-induced spin-crossover characteristics of a functional iron(II) complex at submonolayer coverage on HOPG *J. Phys. Chem. C* **125** 13925–32
- [39] Noll T and Radu F 2016 The mechanics of the VEKMAG experiment *Proc. MEDSI2016, Beam Lines, End Stations and Sample Environments* vol 38 pp 370–3
- [40] Herper H C *et al* 2013 Iron porphyrin molecules on Cu(001): influence of adlayers and ligands on the magnetic properties *Phys. Rev. B* **87** 174425
- [41] Niell A M, Martín C A and Ramia E 2008 Multi-exponential fit of experimental data: a robust method for pore size distribution determination *Ann. Magn. Reson.* **7** 55–73
- [42] Vlček A Jr 2000 The life and times of excited states of organometallic and coordination compounds *Coord. Chem. Rev.* **200–202** 933–77
- [43] Collison D, Garner C D, McGrath C M, Mosselmans J F W, Roper M D, Seddon J M W, Sinn E and Young N A 1997 Soft x-ray induced excited spin state trapping and soft x-ray photochemistry at the iron $L_{2,3}$ edge in $[\text{Fe}(\text{phen})_2(\text{NCS})_2]$ and $[\text{Fe}(\text{phen})_2(\text{NCSe})_2]$ (phen = 1,10-phenanthroline) *J. Chem. Soc., Dalton Trans.* **22** 4371–6
- [44] Kipgen L, Bernien M, Nickel F, Naggert H, Britton A J, Arruda L M, Schierle E, Weschke E, Tuczek F and Kuch W 2017 Soft-x-ray-induced spin-state switching of an adsorbed Fe(II) spin-crossover complex *J. Phys.: Condens. Matter* **29** 394003
- [45] Moliner N *et al* 2002 Thermal and optical switching of molecular spin states in the $[\text{FeL}(\text{H}_2\text{B}(\text{pz})_2)_2]$ spin-crossover system (L = bpy, phen) *J. Phys. Chem. B* **106** 4276–83
- [46] Kumar K S and Ruben M 2021 Sublimable spin-crossover complexes: from spin-state switching to molecular devices *Angew. Chem., Int. Ed.* **60** 7502–21
- [47] Létard J-F 2006 Photomagnetism of iron(II) spin crossover complexes—the T(LIESST) approach *J. Mater. Chem.* **16** 2550–9
- [48] Grunwald J *et al* 2023 Defying the inverse energy gap law: a vacuum-evaporable Fe(II) low-spin complex with a long-lived LIESST state *Chem. Sci.* **14** 7361–80
- [49] Chastanet G, Lorenc M, Bertoni R and Desplanches C 2018 Light-induced spin crossover—solution and solid-state processes *C. R. Chim.* **21** 1075–94
- [50] Juhász G, Hayami S, Sato O and Maeda Y 2002 Photo-induced spin transition for iron(III) compounds with π – π interactions *Chem. Phys. Lett.* **364** 164–70
- [51] Hauser A 1995 Intersystem crossing in iron(II) coordination compounds: a model process between classical and quantum mechanical behaviour *Comments Inorg. Chem.* **17** 17–40
- [52] Hauser A 1991 Intersystem crossing in Fe(II) coordination compounds *Coord. Chem. Rev.* **111** 275–90
- [53] Wang H, Desplanches C, Dagaulta P and Létard J-F 2014 A new family of diamagnetic macrocyclic Fe(II) compounds exhibiting the LIESST effect at high temperatures *Dalton Trans.* **43** 15346–50
- [54] Vela S and Paulsen H 2019 Deciphering crystal packing effects in the spin crossover of six $[\text{Fe}^{\text{II}}(2 - \text{pic})_3]\text{Cl}_2$ solvatomorphs *Dalton Trans.* **48** 1237–45
- [55] McGravey J J and Lawthers I 1982 Photochemically-induced perturbation of the $^1A \leftrightarrow ^5T$ equilibrium in Fe(II) complexes by pulsed laser irradiation in the metal-to-ligand charge-transfer absorption band *J. Chem. Soc., Chem. Commun.* **16** 906–7
- [56] Johannsen S, Ossinger S, Markussen T, Tuczek F, Gruber M and Berndt R 2021 Electron-induced spin-crossover in self-assembled tetramers *ACS Nano* **15** 11770–8
- [57] Johannsen S, Ossinger S, Grunwald J, Herman A, Wende H, Tuczek F, Gruber M and Berndt R 2022 Spin crossover in a cobalt complex on Ag(111) *Angew. Chem., Int. Ed.* **61** 7
- [58] Johannsen S, Schüddekopf S, Ossinger S, Grunwald J, Tuczek F, Gruber M and Berndt R 2022 Three-state switching of an Fe spin crossover complex *J. Phys. Chem. C* **126** 7238–44
- [59] Naggert H, Bannwarth A, Chemnitz S, von Hofe T, Quandt E and Tuczek F 2011 First observation of light-induced spin change in vacuum deposited thin films of iron spin crossover complexes *Dalton Trans.* **40** 6364–6
- [60] Ludwig E, Naggert H, Kalläne M, Rohlf S, Kröger E, Bannwarth A, Quer A, Rosnagel K, Kipp L and Tuczek F 2014 Iron(II) spin-crossover complexes in ultrathin films: electronic structure and spin-state switching by visible and vacuum-UV light *Angew. Chem., Int. Ed.* **53** 3019–23
- [61] Hayami S, Gu Z, Shiro M, Einaga Y, Fujishima A and Sato O 2000 First observation of light-induced excited spin state trapping for an iron(III) complex *J. Am. Chem. Soc.* **122** 7126–7
- [62] Paradis N, Gac F L, Guionneau P, Largeteau A, Yufit D S, Rosa P, Létard J-F and Chastanet G 2016 Effects of internal and external pressure on the $[\text{Fe}(\text{PM} - \text{PEA})_2(\text{NCS})_2]$ spin-crossover compound (with $\text{PM-PEA} = N-(2' - \text{pyridylmethylene})-4-(\text{phenylethynyl})\text{aniline}$) *Magnetochemistry* **2** 17
- [63] Serebryuk M, Muñoz M C, Castro M, Romero-Morcillo T, Gaspar A B and Real J A 2013 Unprecedented multi-stable spin crossover molecular material with two thermal memory channels *Chem. Eur. J.* **19** 6591–6
- [64] Slot T K, Riley N, Shiju N R, Medlin J W and Rothenberg G 2020 An experimental approach for controlling confinement effects at catalyst interfaces *Chem. Sci.* **11** 11024–9
- [65] Rohlf S, Grunwald J, Kalläne M, Kähler J, Diekmann F, Ossinger S, Flöser B, Tuczek F, Rosnagel K and Gruber M

- 2021 Probing the spin state of spin-crossover complexes on surfaces with vacuum ultraviolet angle-resolved photoemission spectroscopy *J. Phys. Chem. C* **125** 14105–16
- [66] Wäckerlin C, Donati F, Singha A, Baltic R, Decurtins S, Liu S-X, Rusponi S and Dreiser J 2018 Excited spin-state trapping in spin crossover complexes on ferroelectric substrates *J. Phys. Chem. C* **122** 8202–8
- [67] Vankó G, Renz F, Molnár G, Neisius T and Kárpáti S 2007 Hard-x-ray-induced excited-spin-state trapping *Angew. Chem., Int. Ed.* **46** 5306–9